Hierarchical Hollow Spheres of ZnO and Zn 1− x Co x O: Directed Assembly and Room-Temperature Ferromagnetism

ARTICLE · JANUARY 2010

CITATIONS
9

READS
23

7 AUTHORS, INCLUDING:

Wei Chen
Chinese Academy of Sciences
874 PUBLICATIONS **13,885** CITATIONS
SEE PROFILE

Xixiang Zhang
King Abdullah University of Science and Tec…
394 PUBLICATIONS **11,653** CITATIONS
SEE PROFILE

Ka Sing Lawrence Wong
The Chinese University of Hong Kong
484 PUBLICATIONS **9,770** CITATIONS
SEE PROFILE

DOI: 10.1021/cg900832m

CRYSTAL GROWTH & DESIGN Article

2010, Vol. 10
177–183

Hierarchical Hollow Spheres of ZnO and $Zn_{1-x}Co_xO$: Directed Assembly and Room-Temperature Ferromagnetism

Yongcai Qiu,[†,‡] Wei Chen,[‡] Shihe Yang,*[,†,‡] B. Zhang,[§] X. X. Zhang,[§] Y. C. Zhong,[§] and K. S. Wong[§]

[†]*Nano Science and Technology Program, The Hong Kong University of Science and Technology, Clear Water Bay, Kowloon, Hong Kong, P. R. China,* [‡]*Department of Chemistry, The Hong Kong University of Science and Technology, Clear Water Bay, Kowloon, Hong Kong, P. R. China, and* [§]*Department of Physics, The Hong Kong University of Science and Technology, Clear Water Bay, Kowloon, Hong Kong, P. R. China*

Received July 18, 2009; Revised Manuscript Received November 2, 2009

ABSTRACT: A novel water-bubble template process has been developed to synthesize uniform hierarchical hollow spheres of ZnO and transition metal doped ZnO in ethylene glycol. For undoped ZnO, nanorods are formed due to the preferred *c*-axial growth and assembled into highly regular hollow spheres. Co-doped ZnO, in contrast, favors lateral growth into nanodisks because of the deterred *c*-axial extension caused by the Co dopants. Nevertheless, the $Zn_{1-x}Co_xO$ (x = ~0.59%, ~1.62%, ~5.21%) nanodisks, albeit with a very different morphology from the nanorods, are also assembled cleanly into high-quality hollow spheres. The synthesis conditions have been carefully studied and the products have been extensively characterized by a variety of techniques. In particular, Raman scattering and photoluminescence spectra of the $Zn_{1-x}Co_xO$ hollow spheres prove that the Co atoms occupy the Zn sites of wurtzite ZnO. Also, room temperature magnetic measurements show robust coercivities, signifying the ferromagnetism that is characteristic of dilute magnetic semiconductors (DMS).

Introduction

The design and construction of hollow micro- or nanostructures have relied on a number of strategies such as the Kirkendall effect,[1,2] Ostwald ripening,[3,4] and hard/soft templates.[5,6] The interest largely arose from the low densities, large surface areas, and high surface permeability of the hollow spheres in comparison with their bulk-phase counterparts. These materials have widely exhibited their potential applications in thermally insulating fillers, composite materials, catalysis, drug delivery, photonic crystals, and sensors.[7−13] The conventional hard-template approach has been the workhorse for synthesizing these materials, including templates of macroporous active carbon,[14] ceramic hollow spheres,[15] and polystyrene (PS) sphere cores.[16] One of the main hassles with the template methods is the need for calcinations or dissolution steps for template removal. In this sense, sols, particularly gas bubbles, are ideal templates for the construction of hollow superstructures due to the straightforward release of the templates.[10,17−19] Indeed, ZnSe hollow spheres were synthesized under hydrothermal conditions using hydrazine as the reducing agent, from which N_2 bubbles were generated and acted as a template.[17,18]

As a low-cost and wide band gap semiconductor, ZnO itself not only has been a focus of interest in studies for near-UV light emitters, transparent high-power electronics, surface acoustic wave devices, piezoelectric transducers, and photoanodes of solar cells[20−25] but also has important applications as emerging dilute magnetic semiconductor (DMS) materials when doped with a small percentage of magnetic impurities.[26] Spintronic devices such as spin-valve transistors, spin light-emitting diodes, optical isolators, and ultrafast optical switches are some of the areas of interest for introducing room-temperature ferromagnetic properties in a semiconductor.[27,28] So far, considerable efforts in these fields have been devoted to the syntheses of transition metal (TM)-doped ZnO DMS thin films, one-dimensional materials, and micro- or nanocrystals using different methods such as pulsed laser deposition (PLD), magnetron cosputtering, chemical vapor deposition (CVD), and sol−gel methods.[29−33] However, there have been very few reports on the synthesis of hollow micro- or nanoscale spherical superstructures of DMS materials in solution phase.[20] Herein, we propose a facile solvothermal process to fabricate ZnO and cobalt(II) metal doped ZnO hollow spheres by simply using water bubbles as a template in ethylene glycol (EG). Unlike surfactants,[34] emulsion droplets,[35] and block copolymers,[36] the use of water bubbles as a soft template for the construction of hollow spheres is expected to considerably simplify the synthesis and ensure the purify of the hollow sphere products. Recently, Zhang et al. synthesized hollow ZnS nanospheres by templating with in situ generated bubbles released from KBH_4 in a water-containing solution.[37] By the generation of water bubbles in EG, for the first time, we are able to achieve the hierarchical assembly of ZnO nanorods and $Zn_{1-x}Co_xO$ nanodisks into uniform hollow spheres. Here by "hierarchical", we mean the existence of different levels of structures. Because EG and water are miscible but with very different boiling points and viscosities, the experimental conditions are easily tunable and controllable. Moreover, we also first demonstrate the DMS-based room-temperature ferromagnetism of the hierarchically assembled $Zn_{1-x}Co_xO$ nanodisk hollow spheres by presenting preliminarily magnetic measurement results at 300 K.

Experimental Section

Preparation of ZnO and Transition Metal Doped ZnO Hollow Spheres. A typical procedure was as follows: Four millimoles of

*To whom correspondence should be addressed. E-mail: chsyang@ust.hk.

Published on Web 12/03/2009

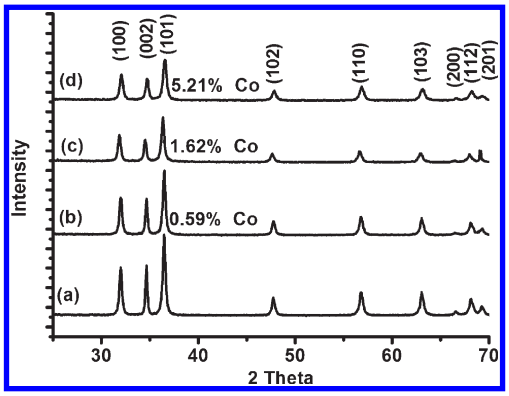

Figure 1. Powder X-ray diffraction patterns of as-prepared pure and three Co-doped ZnO samples.

mixed reactants of zinc acetate dihydrate with or without different amounts of cobalt acetate was dissolved in 4 mL of water with magnetic stirring for 15 min. Sixty milliliters of ethylene glycol was added into the above mixed solution with magnetic stirring for 1 h. Then the mixture was sealed in a Teflon-lined stainless-steel autoclave of 100 mL capacity, kept at 150 °C for 3−5 h, and then allowed to cool to room temperature naturally. White (green for Co-doped ZnO) precipitates were centrifugally collected and rinsed with absolute ethanol several times. Finally, the precipitates were dried in air at 60 °C overnight.

Characterization. The as-prepared products were characterized by scanning electron microscopy (SEM), transmission electron microscopy (TEM), and powder X-ray diffraction (XRD) measurements. Product morphologies were directly examined by SEM using JEOL 6390F and JEOL 6700F at an accelerating voltage of 5 kV. Elemental analysis was conducted on an energy-dispersive X-ray spectrometer (EDS) attached to the JEOL 6390F. For TEM observations, the as-synthesized products were ultrasonically dispersed in ethanol and then dropped onto carbon-coated copper grids. TEM observations were carried out on a JEOL 2010F microscope operating at 200 kV. The XRD analyses were performed on a Philips PW-1830 X-ray diffractometer with Cu Ka radiation (λ = 1.5406 Å) at a scanning speed of 0.025 deg/s over the 2θ range of 10−70°. XPS spectra were measured on a Perkin-Elmer model PHI 5600 XPS system with a resolution of 0.3−0.5 eV from a monochromated aluminum anode X-ray source. The samples were in powder form dispersed on a carbon tape that was attached to a sample holder. The fluorescence spectra were measured using a He−Cd continuous wave laser operated at 325 nm. Raman spectroscopy was performed at room temperature in a Renishaw RM 3000 Micro-Raman system (spectral resolution < 1 cm^{-1}), employing an Ar^+ laser for excitation. Magnetic properties of the obtained hollow spherical samples were investigated with a highly sensitive magnetometer (SQUID, Quantum Design MPMS XL7).

Results and Discussion

In the absence of transition metal doping, the as-synthesized products are nanorod-based hollow sphere assemblies generated by thermolysis of zinc glycolates or alkoxide derivatives in ethylene glycol. From the powder X-ray diffraction pattern in Figure 1a, all diffraction peaks can be ascribed to ZnO in the hexagonal wurtzite phase without contamination from other crystalline phases. Representative field-emission scanning electron microscopy (SEM) and transmission electron microscopy (TEM) images of the as-prepared product are shown in Figure 2. Clearly, the ZnO product is mainly composed of well-defined hollow spherical architectures with an average diameter of 3 μm. Higher-magnification SEM images (Figure 2b−e) show that the shells of these spheres are constructed from a monolayer of oriented nanorods with lengths ranging from 200 to 500 nm. It is noted that all nanorods in these shells are well aligned and have their oriented growth direction perpendicular to the surface of spheres. Close observations of these images indicate that these nanorods have smooth surfaces with diameters ranging from tens to several tens of nanometers. Importantly, the SEM image in Figure 2e further reveals that these nanorods are attached at sharp ends of the nanorod bundles, supporting the oriented attachment assembly mechanism from the nanoparticles. A typical TEM image of nanorod-based spheres is shown in Figure 2f. The darker appearance of the edge portions of these spheres than that of the centers confirms the hollow interiors of the unique nanorod-based superstructure. The high-resolution TEM image of a single-crystalline ZnO nanorods in Figure 2g shows that the nanorod is well-crystallized with (002) fringes running along the nanorod direction and a recognized spacing by 2.6 Å. This is consistent with preferential growth of the nanorod along the *c*-axis direction, as indicated by the arrow in Figure 2g. The HRTEM image of the nanorod also reveals large-scale grain boundaries between the ZnO particles, further corroborating the crystal formation via oriented attachment of these nanoparticles. The oriented growth and the subsequent self-assembly of the ZnO nanorods represent an integral approach for the synthesis of hierarchical hollow structures at widely differing length scales.

We extended the above solvothermal process for pure ZnO products to transition-metal doped ZnO by adding magnetic impurities (e.g., Mn, Fe, Ni) in the starting reactants. This represents a viable alternative for the synthesis of dilute magnetic semiconductor (DMS) materials in a solution system, which has advantages of simplicity and scalability. For illustration here, our report is limited to the cobalt-doped ZnO DMS. In much the same way as in the synthesis of nondoped ZnO above, we have obtained a Co-doped ZnO hollow superstructure but by hierarchical assembly of nanodisks instead of nanorods. Powder X-ray diffraction patterns of the as-prepared products with three levels of cobalt doping are presented in Figure 1b−d. All diffraction peaks are in fairly good agreement with those of standard patterns for the hexagonal wurtzite ZnO (JCPDS card no. 36-1451). The sharp and intense XRD diffraction peaks of all the products show their highly crystalline characteristics. Figure 3 shows SEM, TEM, and energy-dispersive X-ray (EDX) spectroscopic mapping, as well as selected-area electron diffraction (SAED) results of the Co-doped ZnO sample. From low-magnification SEM images (Figure 3a), it can be seen that the products take well-defined spherical architecture with an average diameter of about 3 μm. To verify the morphological characteristics of the samples, we refer to the typical high-magnification SEM images (Figure 3b,c), which manifest that these spheres are constructed by the assembly of the nanometer-sized structures and some fractured spheres display clearly hollow interiors and shells about 500 nm thick. The morphology of the structure is further investigated by TEM. As shown in Figure 3d, the spherical structure is actually constructed from the assembly of nanodisks with widths ranging from tens to several tens of nanometers. The HRTEM image of a nanodisk (Figure 3e) exhibits clear lattice fringes, indicating a high crystallinity of the nanodisk. The recognized lattice spacing of 0.28 nm can be ascribed to the (100) plane of the hexagonal wurtzite ZnO. The corresponding SAED pattern obtained from a single nanodisk (Figure 3f) displays well-defined spots with the zone axis of [001] perpendicular to the nanodisk, indicating the suppression of *c*-axis elongation

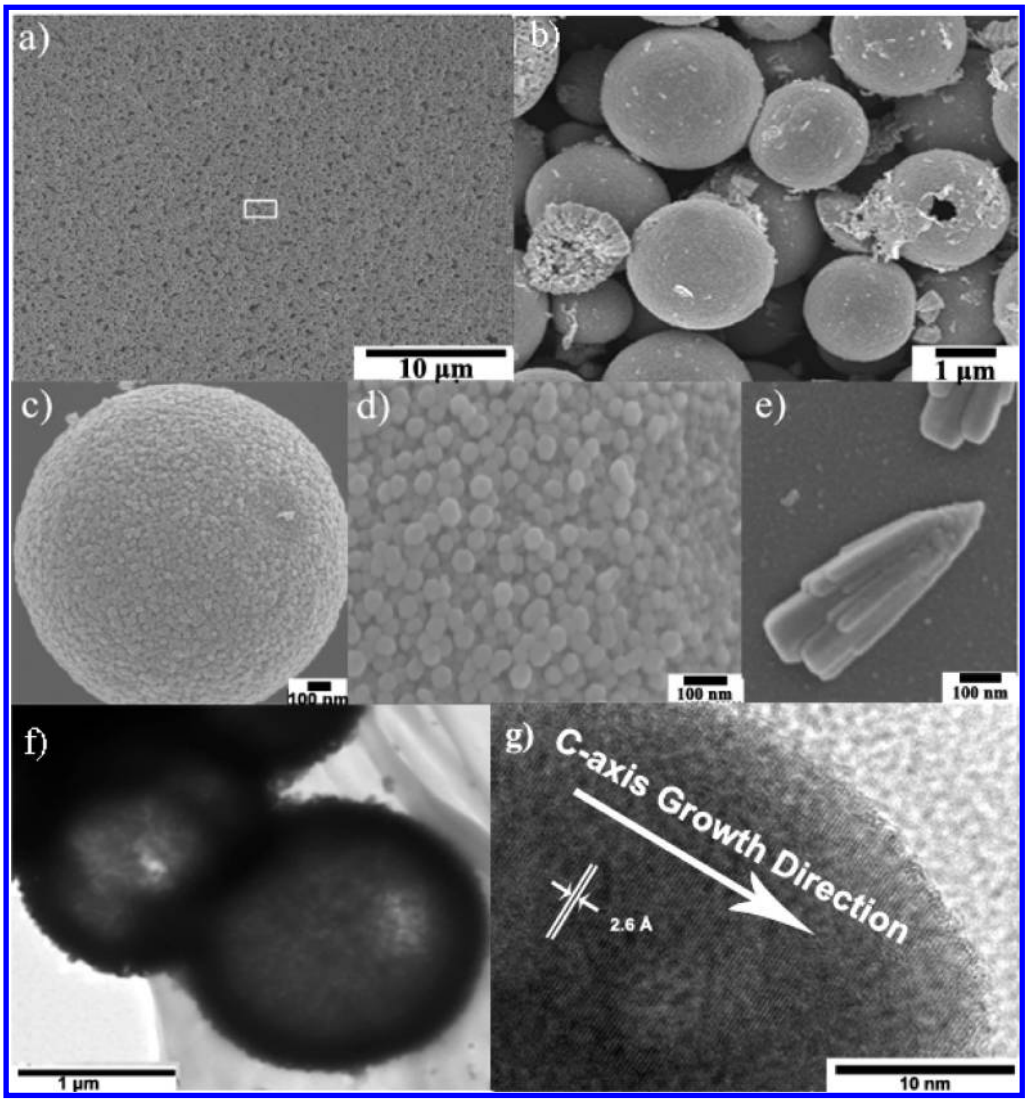

Figure 2. (a) Low-magnification SEM image of as-prepared ZnO hollow spheres, (b) high-magnification SEM image taken from the highlighted section in panel a, (c,d) typical SEM images of an individual superstructure and its surface, (e) representative SEM image from a broken superstructure, (f) TEM image of the as-prepared ZnO hollow spheres, (g) HRTEM image of part of a constituent single nanorod in a hollow sphere.

versus the sideway growth enroute to the ZnO nanodisk morphology. Figure 3h−j shows, respectively, the O, Zn, and Co energy dispersive X-ray (EDX) spectroscopic mapping images. To further estimate the actual cobalt(II) contents in the as-prepared DMS samples, we performed elemental quantification by X-ray photoelectron spectroscopy (XPS). From the XPS spectra in Figure 4, the Co $2p_{3/2}$ core level for the DMS samples has a binding energy of around 780 eV, while the Co $2p_{1/2}$ core level is located at about 795.5 eV. By virtue of the XPS spectra, the cobalt atomic concentrations for the three samples can be estimated to be about 0.59%, 1.62%, and 5.21%, respectively. We also performed SEM EDX analysis (see Supporting Information), and the cobalt atomic concentrations were estimated to be about 0.64%, 1.57%, and 5.19% for the three samples in good agreement with those of the XPS analysis.

We have confirmed that the presence of an appropriate amount of water is crucial for the synthesis of the nanorod-based hollow superstructure. From Figure 5a−c, SEM images show the morphology changes of the as-prepared products with increasing water amount: (a) 0, (b) 2, and (c) 8 mL. When no water was added in the experiment, only colloidal spherical aggregates of ZnO nanoparticles were obtained, as can be seen in Figure 5a. By zooming into an individual spherical aggregate intentionally pared by grinding the sample (see the inset of Figure 5a), it is clear that there is no hollow interior. Upon addition of only 2 mL of water, hollow superstructures could be detected, but with thick shells of > 500 nm as well as many fused multimers (Figure 5b) possibly formed from Brownian-motion-driven particle collisions.[38,39] When 8 mL of water was added, as can be seen from Figure 5c, different nanorod-assembled morphologies of the as-prepared product were observed, indicating that the superfluous water overly promoted the anisotropic growth such that the hollow spheres are easily fractured into an assortment of hierarchical structures. Moreover, control experiments with different reaction temperature from 90 to 180 °C and with different reaction time from 0.5 to 10 h in the experiment with an addition of 4 mL of water showed that precipitates were only observed at reaction temperature over 100 °C. With an increasing reaction temperature or reaction time, there is a small or unnoticeable effect on the morphologies of the ZnO products, but more

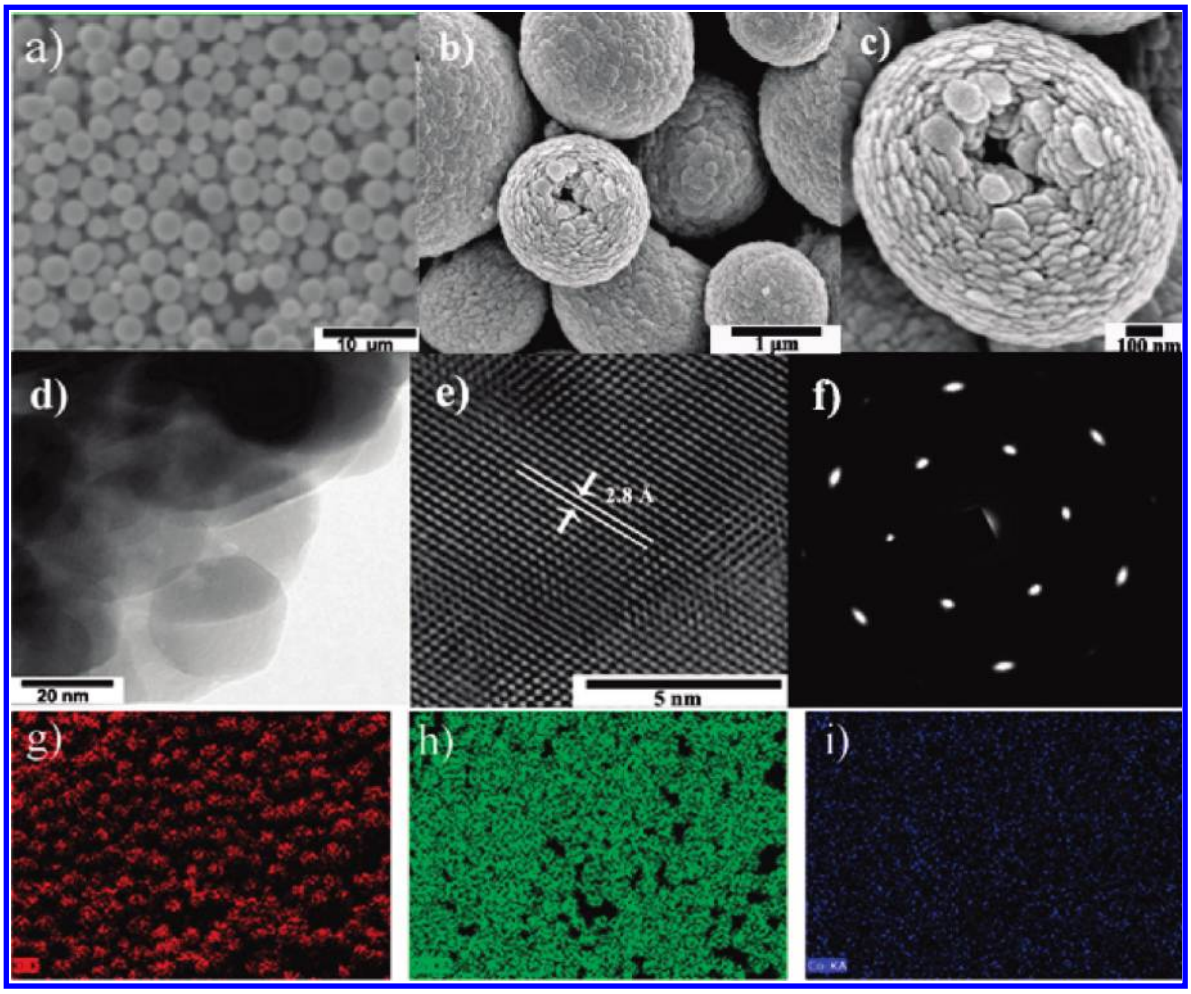

Figure 3. (a, b) Low- and high-magnification SEM images of as-prepared Co-doped ZnO hollow spheres, (c) typical SEM image of an individual Co-doped ZnO hollow sphere, (d−f) typical TEM image, HRTEM image, and SAED pattern of the constituent nanodisks in a Co-doped ZnO hollow sphere, and (g−i) energy-dispersive X-ray (EDX) spectroscopic mapping of as-prepared Co-doped ZnO hollow spheres.

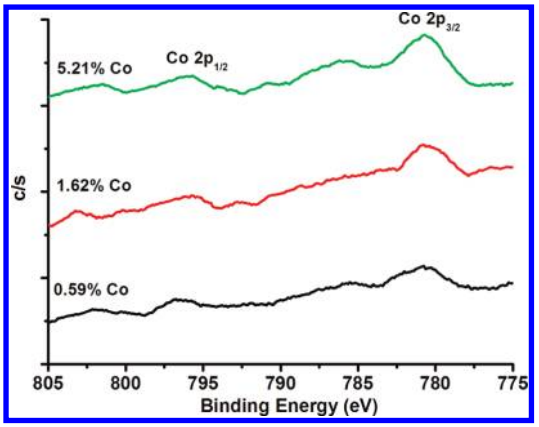

Figure 4. XPS spectra of the three Co-doped ZnO hollow sphere samples showing the Co 2p core-level photoemission.

hollow spheres are cracked. The experiments imply that the formation of these hollow spheres can result from water bubbles.

The results presented above highlight a facile, water bubble-assisted solvothermal process for the growth of nanorod-based hollow spheres. As a well-known wurtzite metal oxide, ZnO exhibits a positive polar (001) plane and a negative polar (00$\bar{1}$) plane, which are rich in Zn and O atoms, respectively. Both polar planes with surface dipoles are thermodynamically unstable and have higher growth rate to reduce their surface energy. It has been reported that the $[Zn(OH)_4]^{2-}$ species prefers to be adsorbed on the positive polar plane by Coulomb interactions, and this facilitate the further nucleation and growth along this direction.[40−43] Ethylene glycol (EG) is a polar solvent with a boiling point of 198 °C and a high permittivity of 37 at 20 °C, which is believed to have high dissolving capacity for polar inorganic materials. Moreover, it is a strong reducing agent and is more viscous and less thermally efficient than pure water. These intrinsic factors may play important roles for the construction of the hollow spheres.

On the basis of the present results, the discussion above, and previous works by others,[20,40−43] a possible mechanism for the formation of ZnO and Co-doped ZnO nuclei and the growth of the hollow superstructures can be proposed in Figure 6. The primary ZnO nuclei formed by thermolysis of zinc glycolates or alkoxide derivatives at a reaction temperature above 100 °C. Meanwhile, water bubbles are generated to provide the assembly centers during the reaction. To minimize the interfacial energy, ZnO nuclei aggregate together around the gas−liquid interface, and finally hollow nanorod-based spheres form through an oriented attachment growth mechanism as mentioned above. For the growth of the nanodisks, we believe that the addition of a small amount of

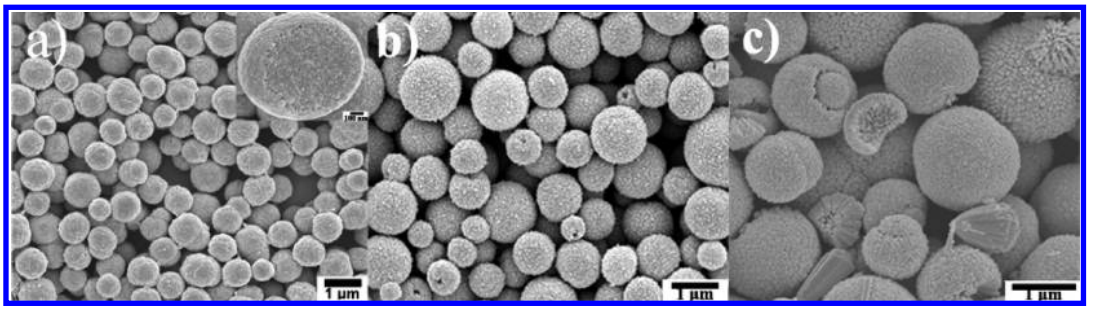

Figure 5. Pure ZnO hollow spheres synthesized using different amounts of water: (a) 0, (b) 2, and (c) 8 mL. Inset of panel a is an enlarged image of a sphere showing the solid interior.

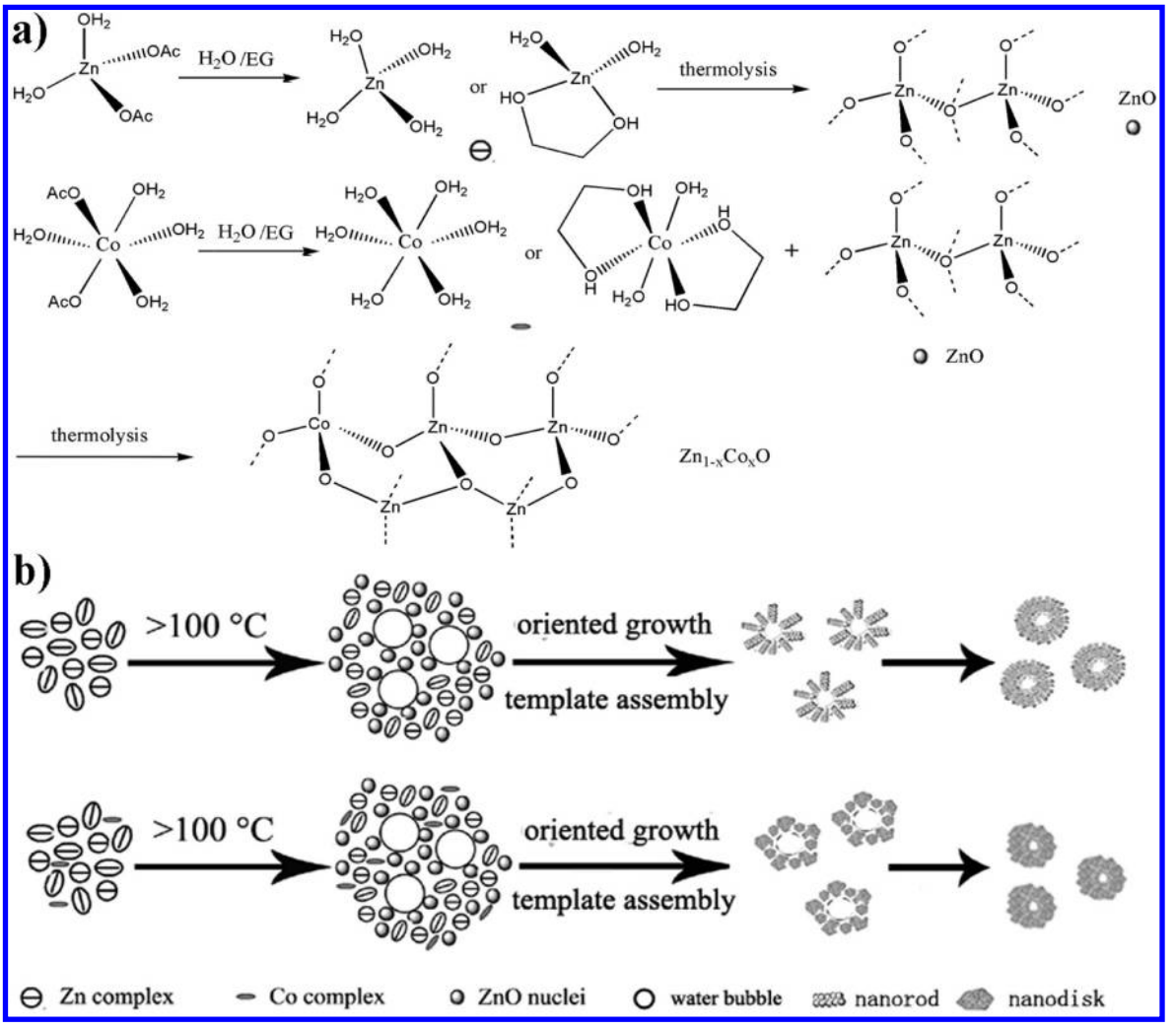

Figure 6. (a) Schematic showing the ZnO and $Zn_{1-x}Co_xO$ formation and (b) the water bubble templated assembly processes of the pure ZnO and Co-doped ZnO hollow spheres.

cobalt(II)−ethylene glycol has played an important role in the self-limiting anisotropic growth of ZnO nanostructures. In the growth process, the cobalt(II) ions have the tendency to adsorb on the O-terminated $(00\bar{1})$ surface of ZnO nuclei, thus obstructing the crystal growth along the [001] direction and leading to the morphological transition to ZnO nanodisks, which are bulk doped uniformly with Co, rather than the formation of undoped ZnO nanorods. Also, it has been shown previously that an as-synthesized cobalt oxide precursor has a preference to form nanoplates by assembling the cobalt(II) ions in ethylene glycol.[44]

The hollow spherical superstructures of four different samples were further investigated by Raman scattering and optical measurements at room temperature. Figure 7 shows the Raman spectra of all four as-prepared products. For the undoped ZnO, the sharpest and strongest peak at about 438 cm^{-1} can be assigned to the high-frequency branch of the E_2 mode [E_2 (high)] of ZnO. The peaks at 332, 381, and 580 cm^{-1} are assigned to the second-order vibration mode [$2E_2$ (low)], the transverse-optical mode with A_1 symmetry [A_1 (TO)], and the longitudinal-optical phonon mode with E_1 symmetry [E_1 (LO)], respectively. In comparison with the Raman spectrum

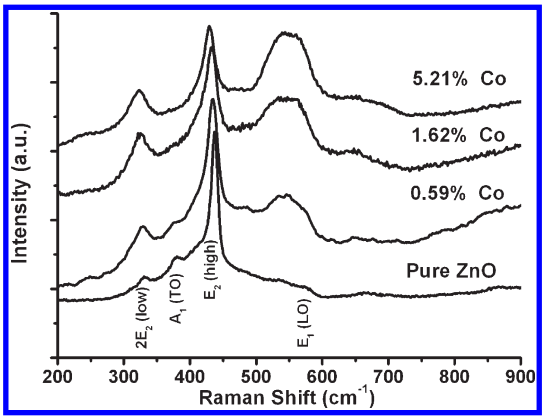

Figure 7. Raman scattering spectra of undoped and Co-doped ZnO hollow spheres excited at the wavelength of 488 nm.

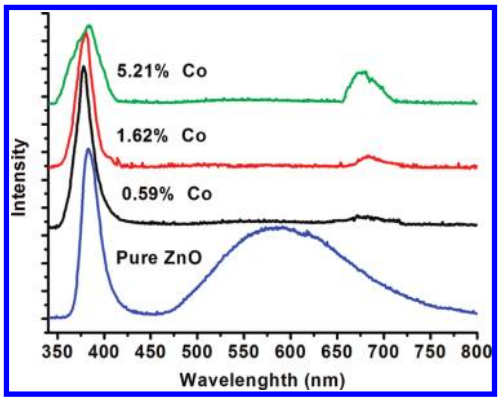

Figure 8. Room-temperature PL spectra of pure ZnO and three different Co-doped ZnO hollow spheres at an excitation wavelength of 325 nm.

of undoped ZnO, the broad bands observed at 500−600 cm^{-1} might be assigned as local vibration of the Co impurities in ZnO matrix.[45−47] Photoluminescence is a very effective method for the investigation of intrinsic point defects in ZnO, such as zinc vacancies, interstitial oxygen, interstitial zinc, and oxygen vacancies. As shown in Figure 8, all four samples exhibit strong near-band-edge (violet) emission peaks around 380 nm, which are associated with zinc vacancy related defects.[48,49] Another relatively broad emission band for the pure ZnO superstructure is in the range of 460−760 nm, peaking at around 570 nm. The green band emission can be ascribed to singly ionized oxygen vacancies in ZnO, and it arises from the radiative recombination of a photogenerated hole with an electron occupying the oxygen vacancy.[50,51] In most cases, however, the violet emission band is accompanied by a yellow−orange band, normally attributed to oxygen interstitials.[52,53] For the Co-doped ZnO samples we measured, however, the broad emission peaks become very weak, a clear indication of the presence of Co^{2+} in the ZnO nanocrystals, which can provide competitive pathways for recombination and therefore nearly completely quench the yellow luminescence. Meanwhile a new weak peak appears at around 680 nm and grows with increasing Co content, and this emission can be ascribed to the $^4T_1(P) \rightarrow {}^4A_2(F)$ transition of Co(II) ion in a tetrahedral crystal field.[54,55] These results further confirm that the Co(II) ions are well located in the Zn(II) sites in the wurtzite ZnO structure, indicating the fairly good solubility of Co(II) ions in ZnO as shown schematically in Figure 9.

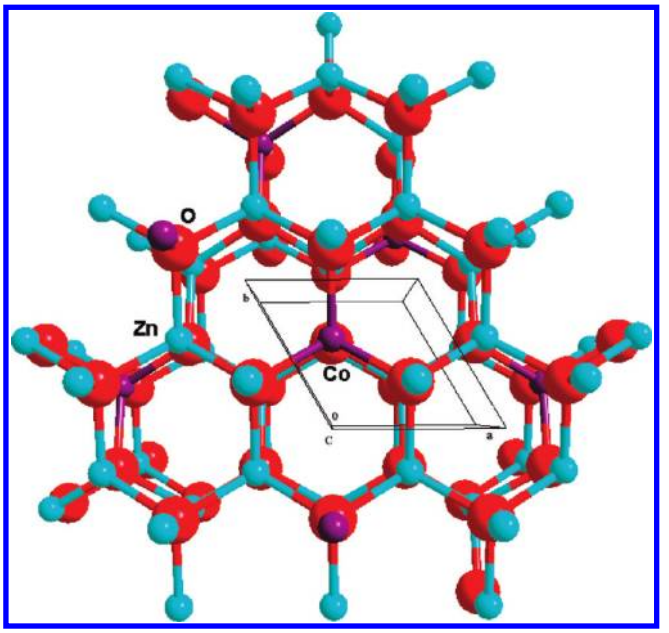

Figure 9. The lattice structure of Co-doped ZnO, in which Co occupies the Zn sites of wurtzite ZnO.

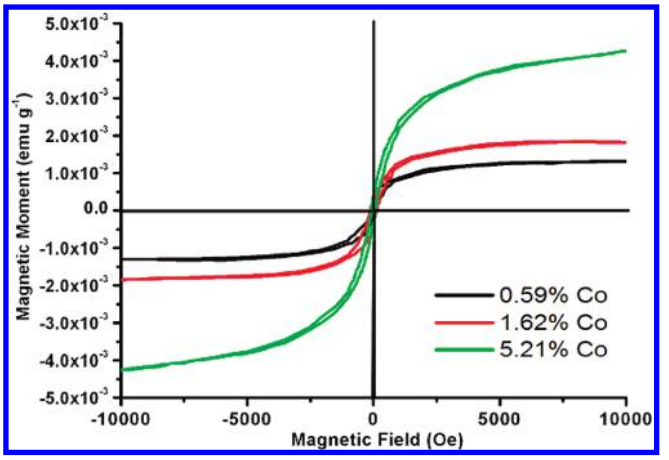

Figure 10. Magnetization versus magnetic field ($M-H$) curves at room temperature (300 K) for three different Co-doped ZnO hollow sphere samples.

Finally, magnetic hysteretic loops for the samples with three levels of Co-doping from SQUID measurements are shown in Figure 10. The magnetization versus magnetic field ($M-H$) loops for the $Zn_{1-x}Co_xO$ (x = ~0.59%, ~1.62%, and ~5.21%) samples at room temperature (300 K) exhibit the coercive field (H_c) of approximately 125, 112, and 95 Oe, respectively. The coercivity decreases with increasing cobalt doping level. However, the saturation magnetization (M_s) values of the three samples were found to increase with increasing cobalt doping. Nevertheless, M_s per cobalt still decreases with increasing content of Co. Similar phenomena have been observed in other DMS materials.[56,57] Indirect interaction among Co(II) centers leads to ferromagnetism, whereas direct interaction among them leads to antiferromagnetism.[58,59] With an increase in Co doping, the average distance between Co(II) ions decreases, resulting in enhancement of the antiferromagnetic contribution. The value of M_s is 0.025 μB/Co for ~0.59% Co doping and 0.012 μB/Co for ~1.62% Co doping, and it decreases to 0.0086 μB/Co for ~5.21% Co doping. The

magnetic moment from the Co(II) ion in a tetrahedral crystal field is expected to be 3 μB/Co atom. The rather small value of M_s per Co atom indicates that only a small portion of Co(II) species are contributing to the ferromagnetism and that a significant paramagnetic fraction of Co(II) ions remains.

Conclusion

In conclusion, the water bubble template in a water−ethylene glycol system is an effective method to assemble hollow DMS materials with tempting hierarchical structures. Here the synthesis and assembly of nanostructures are combined and executed in parallel. Two examples have been demonstrated for the hollow spheres: (1) assembled from ZnO nanorods; (2) assembled from $Zn_{1-x}Co_xO$ nanoplates. The latter has been demonstrated to display room-temperature ferromagnetism in this work. Compared with other templated synthetic approaches, this method is advantageous in that it simplifies the fabrication of hollow structures by leaving out the painful step of removing the templates such as surfactants and polymeric spheres. Therefore, this interesting and cost-effective synthetic approach, with template-directed assembly and oriented attachment growth, bodes well for large-scale production.

Acknowledgment. This work was supported by the Hong Kong Research Grants Council (RGC) General Research Funds (GRF) No. HKUST 604107.

Supporting Information Available: SEM EDX spectra of three as-prepared Co-doped ZnO samples with different levels of doping. This material is available free of charge via the Internet an http://pubs.acs.org.

References

(1) Yin, Y. D.; Rioux, R. M.; Erdonmez, C. K.; Hughes, S.; Somorjai, G. A.; Alivisatos, A. P. *Science* **2004**, *304*, 711.
(2) Qiu, Y. F.; Yang, S. H. *Nanotechnology* **2008**, *19*, 265606.
(3) Wang, W. S.; Zhen, L.; Xu, C. Y.; Yang, L.; Shao, W. Z. *J. Phys. Chem. C* **2008**, *112*, 19390.
(4) Li, J.; Zeng, H. C. *J. Am. Chem. Soc*. **2007**, *129*, 15839.
(5) Zhou, G. W.; Chen, Y. J.; Yang, J. H.; Yang, S. H. *J. Mater. Chem*. **2007**, *17*, 2839.
(6) Chen, Q. D.; Shen, X. H.; Gao, H. C. *J. Colloid Interface Sci*. **2007**, *312*, 272.
(7) Caruso, F.; Caruso, R. A.; Mohwald, H. *Science* **1998**, *282*, 1111.
(8) Kim, S. W.; Kim, M.; Lee, W. Y.; Hyeon, T. *J. Am. Chem. Soc*. **2002**, *124*, 7642.
(9) Koo, H. J.; Kim, Y. J.; Lee, Y. H.; Lee, W. I.; Kim, K.; Park, N. G. *Adv. Mater*. **2008**, *20*, 195.
(10) Li, X. X.; Xiong, Y. J.; Li, Z. Q.; Xie, Y. *Inorg. Chem*. **2006**, *45*, 3493.
(11) Li, H. X.; Bian, Z. F.; Zhu, J.; Zhang, D. Q.; Li, G. S.; Huo, Y. N.; Li, H.; Lu, Y. F. *J. Am. Chem. Soc*. **2007**, *129*, 8406.
(12) Zhang, H. G.; Zhu, Q. S.; Zhang, Y.; Wang, Y.; Zhao, L.; Yu, B. *Adv. Funct. Mater*. **2007**, *17*, 2766.
(13) Sokolova, V.; Epple, M. *Angew. Chem., Int. Ed*. **2008**, *47*, 1382.
(14) Lei, Z. B.; Li, J. M.; Ke, Y. X.; Zhang, Y. G.; Zhang, H. C.; Li, F. Q.; Xing, J. Y. *J. Mater. Chem*. **2001**, *11*, 2930.
(15) Chah, S.; Fendler, J. H.; Yi, J. *J. Colloid Interface Sci*. **2002**, *250*, 142.
(16) Han, S. B.; Shi, X. Y.; Zhou, F. M. *Nano Lett*. **2002**, *2*, 97.
(17) Peng, Q.; Dong, Y.; Li, Y. D. *Angew. Chem., Int. Ed*. **2003**, *42*, 3027.
(18) Jiang, C. L.; Zhang, W. Q.; Zou, G. F.; Yu, W. C.; Qian, Y. T. *Nanotechnology* **2005**, *16*, 551.
(19) Wu, C. Z.; Xie, Y.; Lei, L. Y.; Hu, S. Q.; OuYang, C. Z. *Adv. Mater*. **2006**, *18*, 1727.
(20) Zhang, X. L.; Qiao, R.; Kim, J. C.; Kang, Y. S. *Cryst. Growth Des*. **2008**, *8*, 2609.
(21) Tian, Z. R.; Voigt, J. A.; Liu, J.; Mckenzie, B.; Mcdermott, M. J.; Rodriguez, H.; Konishi, M. A.; Xu, H. F. *Nat. Mater*. **2003**, *2*, 821.
(22) Pang, Z. W.; Dai, Z. R.; Wang, Z. L. *Science* **2001**, *291*, 1947.
(23) Govender, K.; Boyle, D. S.; O' Brien, P.; Binks, D.; West, D.; Coleman, D. *Adv. Mater*. **2002**, *14*, 1221.
(24) Huang, M. H.; Mao, S.; Feick, H.; Yan, H. Q.; Wu, Y. Y.; Kind, H.; Weberm, E.; Russo, R.; Yang, P. D. *Science* **2001**, *292*, 1897.
(25) Wang, Z. L.; Song, J. H. *Science* **2006**, *312*, 242.
(26) Bauer, C.; Boschloo, G.; Mukhtar, E.; Hagfeldt, A. *J. Phys. Chem. B* **2001**, *105*, 5585.
(27) Ohno, H. *Science* **1998**, *281*, 951.
(28) Dietl, T.; Ohno, H.; Matsukura, F.; Cibert, J.; Ferrand, D. *Science* **2000**, *287*, 1019.
(29) Schwartz, D. A.; Kittilstved, K. R.; Gamelin, D. R. *Appl. Phys. Lett*. **2004**, *85*, 1395.
(30) Khare, N.; Kappers, M. J.; Wei, M.; Blamire, M. G.; MacManus-Driscoll, J. L. *Adv. Mater*. **2006**, *18*, 1449.
(31) Nakayama, M.; Tanaka, H.; Masuko, K.; Fukushima, T.; Ashida, A.; Fujimura, N. *Appl. Phys. Lett*. **2006**, *88*, 241908.
(32) He, J. H.; Lao, C. S.; Chen, L. J.; Davidovic, D.; Wang, Z. L. *J. Am. Chem. Soc*. **2005**, *127*, 16376.
(33) Yuhas, B. D.; Zitoun, D. O.; Pauzauskie, P. J.; He, R.; Yang, P. *Angew. Chem., Int. Ed*. **2006**, *45*, 420.
(34) Zheng, X. W.; Xie, Y. L.; Zhu, Y.; Jiang, X. C.; Yan, A. H. *Ultrason. Sonochem*. **2002**, *9*, 311.
(35) Collins, A. M.; Spickermann, C.; Mann, S. *J. Mater. Chem*. **2003**, *13*, 1112.
(36) Ma, Y. R.; Qi, L. M.; Ma, J. M.; Cheng, H. M. *Langmuir* **2003**, *19*, 4040.
(37) Zhang, H.; Zhang, S.; Pan, S.; Li, G.; Hou, J. G. *Nanotechnology* **2004**, *15*, 945.
(38) Yin, Y. D.; Lu, Y.; Xia, Y. N. *J. Am. Chem. Soc*. **2001**, *123*, 771.
(39) Liddell, C. M.; Summers, C. J. *Adv. Mater*. **2003**, *15*, 1715.
(40) Ayudhya, S. K. N.; Tonto, P.; Mekasuwandumrong, O.; Pavarajarn, V.; Praserthdam, P. *Cryst. Growth Des*. **2006**, *6*, 2446.
(41) Mo, M.; Yu, J. C.; Zhang, L.; Li, S. A. *Adv. Mater*. **2005**, *17*, 756.
(42) Zhang, H.; Yang, D.; Li, D.; Ma, X.; Li, S.; Que, D. *Cryst. Growth Des*. **2005**, *5*, 547.
(43) Zeng, Y.; Zhang, T.; Wang, L.; Wang, R.; Fu, W.; Yang, H. *J. Phys. Chem. C* **2009**, *113*, 3442.
(44) Chen, Y. C.; Hu, L.; Wang, M.; Min, Y. L.; Zhang, Y. G. *Colloids Surf., A* **2009**, *336*, 64.
(45) Phan, T. L.; Vincent, R.; Cherns, D.; Nghia, N. X.; Ursaki, V. V. *Nanotechnology* **2008**, *19*, 475702.
(46) Samanta, K.; Dussan, S.; Katiyar, R. S.; Bhattacharya, P. *Appl. Phys. Lett*. **2007**, *90*, 261903.
(47) Wang, X. F.; Xu, J. B.; Zhang, B.; Yu, H. G.; Wang, J.; Zhang, X. X.; Yu, J. G.; Li, Q. *Adv. Mater*. **2006**, *18*, 2476.
(48) Kohan, A. F.; Ceder, G.; Morgan, D.; Van de Walle, C. G. *Phys. Rev. B* **2000**, *61*, 15019.
(49) Erhart, P.; Albe, K.; Klein, A. *Phys. Rev. B* **2006**, *73*, 205203.
(50) Qiu, Y. F.; Yang, S. H. *Adv. Funct. Mater*. **2007**, *17*, 1345.
(51) Cheng, H. M.; Hsu, H. C.; Tseng, Y. K.; Lin, L. J.; Hsieh, W. F. *J. Phys. Chem. B* **2005**, *109*, 8749.
(52) Jeong, S. H.; Kim, B. S.; Lee, B. T. *Appl. Phys. Lett*. **2003**, *82*, 2625.
(53) Hua, G.; Zhang, Y.; Ye, C.; Wang, M.; Zhang, L. *Nanotechnology* **2007**, *18*, 145605.
(54) Ferguson, J.; Wood, D. L.; Van Uitert, L. G. *J. Chem. Phys*. **1969**, *51*, 2904.
(55) Schulz, H.-J.; Thiede, M. *Phys. Rev. B* **1987**, *35*, 18.
(56) Venkatesan, M.; Fitzgerald, C. B.; Lunney, J. G.; Coey, J. M. D. *Phys. Rev. Lett*. **2004**, *93*, 177206.
(57) MacManus-Driscoll, J. L.; Khare, N.; Liu, Y.; Vickers, M. E. *Adv. Mater*. **2007**, *19*, 2925.
(58) Dietl, T.; Ohno, H.; Matsukura, F.; Cibert, J.; Ferrand, D. *Science* **2000**, *287*, 1019.
(59) Coey, J. M. D.; Venkatesan, M.; Fitzgerald, C. B. *Nat. Mater*. **2005**, *4*, 173.